NANO LETTERS

Letter

pubs.acs.org/NanoLett

Deformation Twinning of a Silver Nanocrystal under High Pressure

Xiaojing Huang,[*,†,‡] Wenge Yang,[*,§,‡] Ross Harder,[∥] Yugang Sun,[⊥] Ming Lu,[#] Yong S. Chu,[†] Ian K. Robinson,[▽,¶] and Ho-kwang Mao[§,△]

[†]National Synchrotron Light Source II and [#]Center for Functional Nanomaterials, Brookhaven National Laboratory, Upton, New York 11973, United States

[‡]HPSynC, Geophysical Laboratory, Carnegie Institution of Washington, Argonne, Illinois 60439, United States

[§]Center for High Pressure Science and Technology Advanced Research, Shanghai 201203, China

[∥]Advanced Photon Source and [⊥]Center for Nanoscale Materials, Argonne National Laboratory, Argonne, Illinois 60439, United States

[▽]London Centre for Nanotechnology, University College London, London, WC1H 0AH, United Kingdom

[¶]Research Complex at Harwell, Didcot, Oxfordshire OX11 0DE, United Kingdom

[△]Geophysical Laboratory, Carnegie Institution of Washington, Washington, DC 20015, United States

Supporting Information

ABSTRACT: Within a high-pressure environment, crystal deformation is controlled by complex processes such as dislocation motion, twinning, and phase transitions, which change materials' microscopic morphology and alter their properties. Understanding a crystal's response to external stress provides a unique opportunity for rational tailoring of its functionalities. It is very challenging to track the strain evolution and physical deformation from a single nanoscale crystal under high-pressure stress. Here, we report an in situ three-dimensional mapping of morphology and strain evolutions in a single-crystal silver nanocube within a high-pressure environment using the Bragg Coherent Diffractive Imaging (CDI) method. We observed a continuous lattice distortion, followed by a deformation twining process at a constant pressure. The ability to visualize stress-introduced deformation of nanocrystals with high spatial resolution and prominent strain sensitivity provides an important route for interpreting and engineering novel properties of nanomaterials.

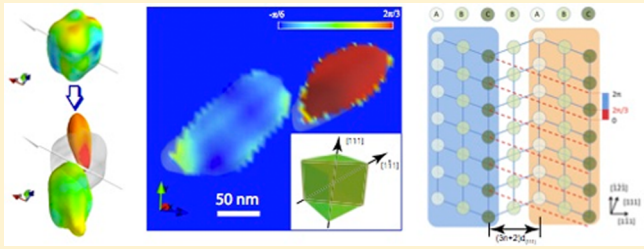

KEYWORDS: *Nanocrystal, deformation twinning, coherent diffractive imaging, X-ray imaging*

Applying controllable high-pressures to materials introduces an additional dimension into a material's phase diagram and enriches its physical and chemical characteristics. Tremendous novel properties[1−3] and new forms of materials[4] have been revealed exclusively under high-pressure. Measuring and understanding the internal strain changes in response to the external pressure produces critical information to unveil the origin of unconventional behavior of crystalline materials in high-pressure environments.

Nanocrystals show abnormal properties compared to their bulk counterparts.[5,6] Explosive growth in the research on nanoscale single crystals has driven the exploration of size-dependent novel mechanical behavior.[7] For example, normal dislocation activity is suppressed in nanocrystals by their high strength and hardness and is replaced by unique plastic deformation that differs from that in coarse-grained materials.[8,9] The deformation of nanocrystals has been investigated in 1D nanowires,[10] 2D nanofilms,[9] and nanopillars attached to a substrate,[7] by applying point-contact stress through nano-indentation. So far, no deformation study on freestanding nanocrystals embedded in an enclosed external stress environment has been reported yet. Bragg CDI offers a unique capability to image the shape and the lattice distortion field inside nanocrystals with high spatial resolution and high strain sensitivity. This method collects a 3D diffraction intensity distribution, commonly called a fringe pattern, in the vicinity of a Bragg peak $\mathbf{Q}$. The fringe spacing carries information on the crystal shape, and the distribution of diffraction power encodes the lattice distortion map.[11] The measured 3D diffraction intensity can be phase-retrieved to give a complex-valued real-space image, wherein the amplitude represents the Bragg electron density and the phase is determined by the lattice dislocation projected onto the momentum transfer vector $\mathbf{Q}$.[12] Recently, the strain and morphology evolutions of a 400 nm sized gold nanocrystal under various high-pressure conditions in a diamond anvil cell (DAC) were successfully visualized using Bragg CDI measurement.[13] Here, we use this same technique to image the stress-induced deformation process of a

Received: September 4, 2015
Revised: October 10, 2015
Published: October 20, 2015

DOI: 10.1021/acs.nanolett.5b03568
Nano Lett. 2015, 15, 7644−7649

single crystal silver nanocube with the edge length about 100 nm, sealed in a panoramic DAC.

In this work, we used water as the pressure transmitting medium. Water provides an ideal enclosure environment for the nanocrystals. Liquid water molecule transforms to a solid state at a relatively low pressure (~0.9 GPa) at room temperature.[14−16] After the water is solidified, it significantly constrains the degrees of freedom of sample motion, both translational and rotational,[17,18] which is critical to allow high-resolution 3D Bragg CDI data acquisition.

The single-crystal silver nanocubes imaged in this experiment were synthesized from ethylene glycol solution of silver nitrate in the presence of poly(vinylpyrrolidone) (PVP).[19] Figure 1

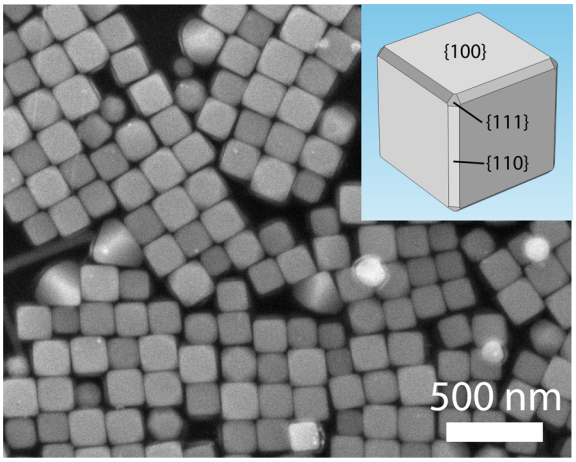

Figure 1. SEM image of silver nanocubes synthesized via the polyol process. The mean edge length is about 120 nm. Each nanocube is mainly confined by {100} planes on the surface, the cubes' edges are truncated to {110} facets, and the corners form small {111} facets (inset).

shows a scanning electron microscope (SEM) picture of these silver nanocubes. The crystals are mainly confined by six {100} planes on their surface, the edges are truncated to {110} facets, and the corners form small {111} facets, as illustrated in the inset of Figure 1. Silver nanocubes with a 120 nm mean edge length were used in this experiment. Upon the initial sealing of the DAC, the pressure was stabilized at 1.5 GPa.

The Bragg CDI measurement was performed at Beamline 34-ID-C of the Advanced Photon Source at Argonne National Laboratory. The DAC, loaded with silver nanocubes, was mounted at the rotation center of the diffractometer. A 9.0 keV coherent X-ray beam, selected by silicon (111) double-crystal monochromator, was focused by a pair of K−B mirrors down to about 1.5 μm.[20] The incident X-rays penetrated the beryllium gasket and illuminated the samples. A direct-detection charge-coupled device (CCD) with 20 μm × 20 μm pitch was placed 0.7 m away from the DAC and oriented to select a silver (111) Bragg peak.

Although the water sealed inside DAC was expected to be in a solid Ice-VI phase at 1.5 GPa,[14−16] we observed significant drifting and rotation of these nanocubes through tracking Bragg peak positions on the CCD detector. The Ice-VI phase was reported to have a finite viscosity, which decreases to the minimum value at the triple point of Ice-VI and Ice-VII.[21] The relatively low viscosity under our measurement condition apparently allowed the nanocubes to move and/or rotate inside Ice-VI environment. We observed that some silver (111) Bragg peaks brightened or dimmed, which is a signature of the sample drifting in and out of the X-ray beam, and some Bragg peaks traveled along the silver (111) Debye−Scherrer ring or rocked across the Bragg peak center, indicating that the crystal spun along different axes.[18] We recorded the Bragg peak positions with sequential X-ray exposures under various pressure conditions. The drifted distances of Bragg peaks on the CCD detector are shown in Figure 2a. At 1.5 and 1.8 GPa, the Bragg

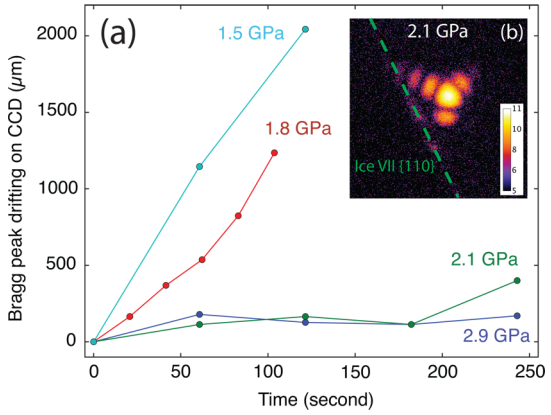

Figure 2. Bragg peak stability at various pressures. (a) Silver (111) Bragg peak drifting was recorded by the CCD detector. The drifting rate slowed down with increasing pressure. With our experimental setup, a drifting of 500 μm on CCD along the Debye−Scherrer ring is equivalent to about a 0.04 degree rotation. (b) A typical silver (111) Bragg peak from a nanocube measured at 2.1 GPa shown in logarithmic scale, in the vicinity of the Ice-VII {110} powder ring.

disappeared on the CCD within 2 min of X-ray illumination. At 2.1 GPa, the Ice-VI phase started to transform to a high-density Ice-VII phase,[22] and the mobility of crystals was significantly slowed down. When we increased the pressure to 2.9 GPa, the nanocrystals became stabilized. However, under this pressure level, the silver nanocrystals were aggressively deformed which destroyed the shapely form facets, as a result no interference fringes could be observed (shown in Figure S1).

Among the four examined pressure conditions, 2.1 GPa provided an optimized combination of sample stability and desired morphology (shown in Figure 2b) for 3D Bragg CDI data collection. However, not all crystals were stabilized under 2.1 GPa. We found that crystals moved rapidly when their orientation satisfied the Bragg condition, while the ones which were slightly off the Bragg peak and held their position reasonably well up to about 10 min (shown in Figure S2). This observation implies that the momentum transfer introduced by Bragg diffraction was the dominant driving force on these silver nanocubes. The relatively slow migration of the Bragg peak at 2.1 GPa also suggested that the crystal underwent a continuous deformation process, as was verified by repeated measurements.

We measured a sequence of Bragg CDI diffraction patterns from a (111) peak of a silver nanocube under a 2.1 GPa pressure environment. The 3D diffraction data covered a 0.4° angular range with 0.02° angular steps. The CCD pixels were 4 × 4 binned to increase the signal statistics. To collect high resolution data within a moderate time interval, each frame was accumulated with three 10 s exposures. The entire data acquisition process took about 10 min within the time range when the nanocubes were still stable. The final cropped array were zero-padded to 96 × 96 × 64 to enhance the image quality through a super-resolution mechanism using a maximum

DOI: 10.1021/acs.nanolett.5b03568
Nano Lett. 2015, 15, 7644−7649

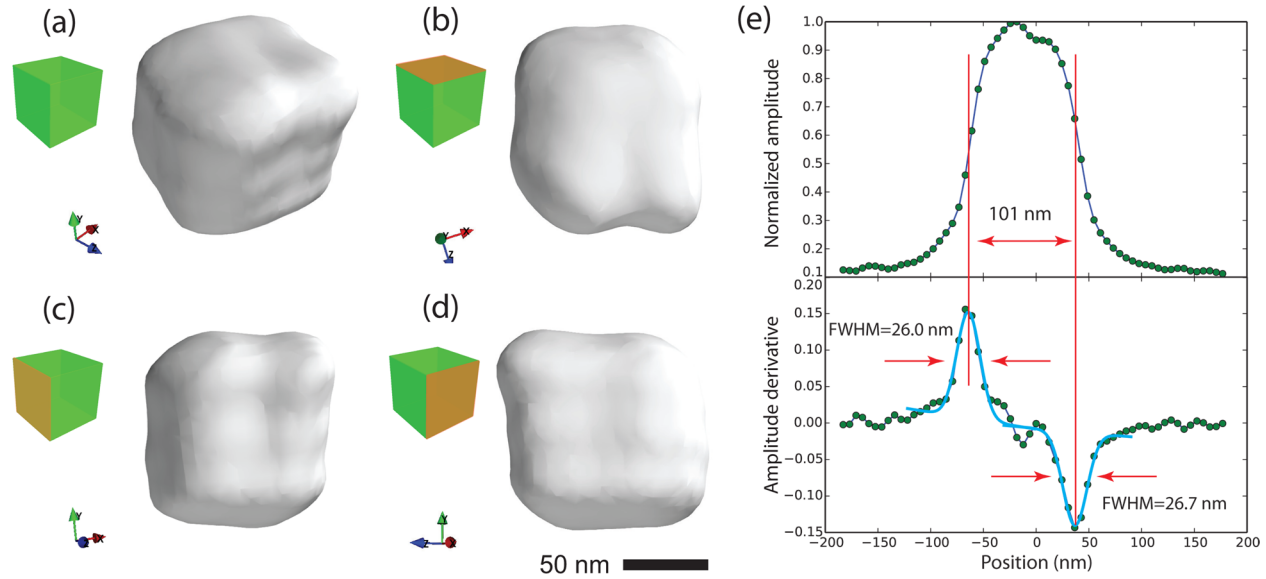

Figure 3. Isosurfaces of the reconstructed nanocube. (a–d) The isometric, top, and side views of the isosurface (20% of the maximum amplitude). (e) Averaged line profile along the vertical direction and its derivative show that the size of the silver nanocube is 101 nm, and the reconstruction resolution is about 27 nm.

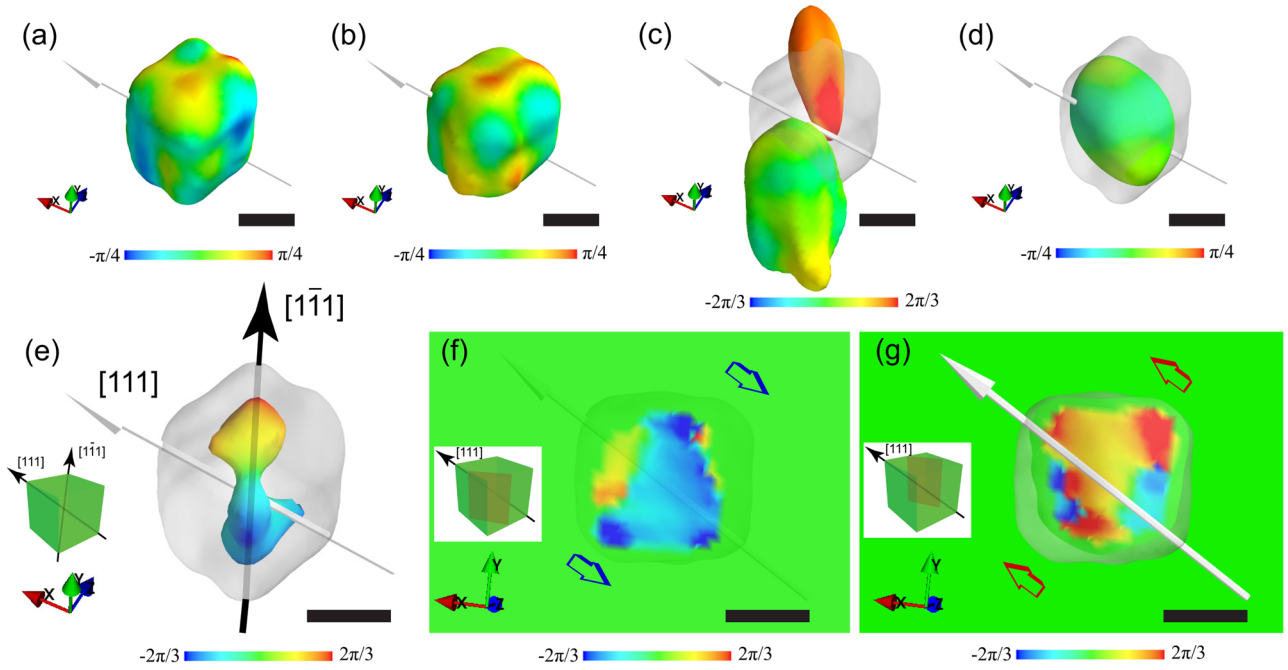

Figure 4. Strain and morphology evolution of the silver nanocube under 2.1 GPa pressure in four sequential measurements. (a–d) The top view of the reconstructed phases from these measurements shown on a 20% amplitude isosurface. The arrow points along the measured [111] direction. (e) The difference Fourier density, superimposed on the amplitude image of (a) with color representing its phase, indicates an expansion trend along the [1$\bar{1}$1] direction. (f and g) Two ($\bar{1}$10) cut-planes of the calculated difference phases indicate distortion fields along opposite directions on the different sides of the silver nanocube. The scale bar is 50 nm.

entropy method.[23] The zero-padded data gave a real space voxel size of 6 × 6 × 6 nm^3.[24]

The *d*-spacing of the silver {111} planes is 2.359 Å, which is very close to the {110} *d*-spacing of the high-density Ice-VII phase (2.362 Å).[22] The powder ring of Ice-VII polycrystal was located in the vicinity of the silver (111) peak, as shown in Figure 2b. The signal from the ice powder ring was masked out before feeding the data into the reconstruction algorithm. The phase retrieval process was started with 40 error-reduction (ER) iterations,[25,26] followed by 420 iterations of the hybrid–input–output (HIO) algorithm,[27] and finished with another 40 ER iterations. The support constraint was refined with the shrink-wrap method.[28] Partial coherence deconvolution[29] was utilized to decompose artifacts from incoherent scattering sourced from upstream optics and adjacent sample environments.[13] Figure 3a–d shows the reconstructed magnitude of the silver nanocube. The obtained crystal size was about 101 nm. Figure 3e plots the central line along the vertical direction, and its derivative on its ascending and descending sides were

DOI: 10.1021/acs.nanolett.5b03568
Nano Lett. 2015, 15, 7644–7649

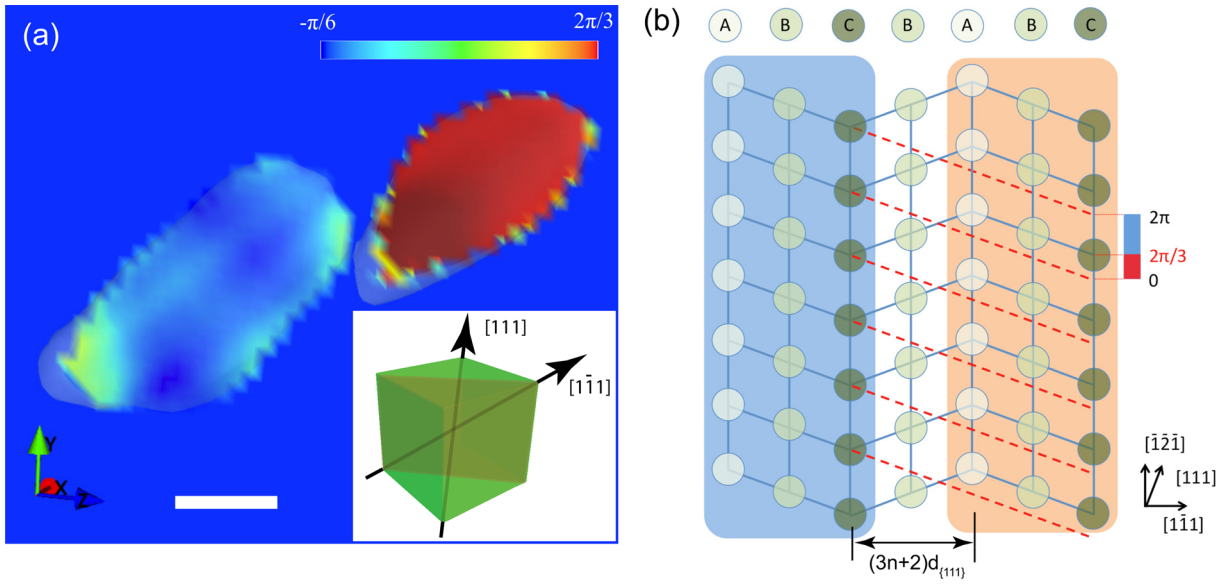

Figure 5. High-pressure introduced deformation twinning in a nanocrystal. (a) The central (110) cutplane of the obtained phase image reconstructed from the third measurement at 2.1 GPa pressure shows a ~$2/3\pi$ phase offset in the detached piece relative to the parent crystal. The scale bar is 50 nm. (b) The deformation twinning separated by $(3n + 2)d_{\{111\}}$ along the [1$\bar{1}$1] direction introduces a $2/3\pi$ phase offset observable on the [111] direction. The twinning section between two parent domains contains a rotated crystalline orientation and thus leaves the missing electron density in the Bragg CDI measurement.

fitted with a Gaussian function, giving fwhm widths of 26.0 and 26.7 nm, respectively.

To track the continuing strain and morphology developments on the same nanocrystal, we repeated the identical measurements in 15, 45, and 75 min. Figure 4a–d shows all reconstructed images from these repeated measurements. In the first measurement (Figure 4a), relatively strong phase features are evident at the cube corners and edges of the crystal. This phase pattern was slightly evolved after 15 min (Figure 4b), with roughly the same distribution but reduced phase values. It suggests that the strain level was decreasing during crystal deformation, which is consistent with previous observations on gold nanocrystals.[13] Since the first two reconstructed images differ only slightly in small regions, the localized difference will be widely spread in reciprocal space. We utilized the difference Fourier technique[30] to identify these subtle changes, with the assumption that the differences are negligible in the recovered reciprocal-space phases.[31] The difference Fourier density $\Delta\rho$ is the Fourier transform of the product of the difference in diffraction amplitudes $[I_{1,2}(q)]^{1/2}$ and the common Fourier phase function $\phi(q)$:

$$\Delta\rho(\mathbf{r}) = \mathrm{FT}\{[\sqrt{I_1(\mathbf{q})} - \sqrt{I_2(\mathbf{q})}]e^{i\phi(\mathbf{q})}\} \quad (1)$$

The calculated difference Fourier density is a complex-valued map, where the amplitude locates the places of the electron density changes and the phase represents the direction of these changes. In Figure 4e, the calculated difference Fourier density between the first two measurements (Figure 4a,b) shows two lobes well aligned along the [1$\bar{1}$1] direction. These difference Fourier density lobes are located near the center of the silver nanocube, which implies that the deformation was initiated in the crystal core. The lobes are displayed with the difference Fourier phases coating their surfaces, which display a symmetric pair of forward and backward displacements with respect to the **Q** vector, similar to those seen in a previous study.[31] This opposite phase distribution indicates that the central region of this silver nanocube was experiencing a radial expansion with respect to the rest of the crystal,[12] as shown in Figure 4f and g.

With the maximum reconstructed amplitude of the first two measurements (shown in Figure 4a and b) scaled as 100 units, the maximum value of the calculated difference Fourier map $|\Delta\rho|$ is 18 ± 1 units, which indicates a phase rotation of 0.18 ± 0.01 radians between the first two measurements[30,31] (also shown in Figure S5). The lattice displacement **u** can be calculated as $|\mathbf{u}| \cos\theta = d{\cdot}\phi/2\pi$, where d is the lattice spacing between {111} planes. Surrounded by the solidified Ice-VII polycrystals, the silver nanocubes were embedded in an anisotropic pressure environment. The corresponding shear stress σ can be estimated as $\sigma = G|\mathbf{u}|/d$,[32] where G is the shear modulus of the silver nanoparticle. Using θ = 70.53°, the measured ϕ value of 0.18 ± 0.01 and the typical shear modulus of silver 30 GPa,[33] the estimated shear stress is about 2.58 ± 0.14 GPa, which is very close to 2.1 GPa given by the Ruby fluorescence measured at a different location. This shear stress significantly exceeded the theoretical elastic limit of shear strength ~1 GPa for silver.[34]

Under such an intensive external shear stress, the silver nanocrystal cannot hold its morphology but develops a plastic deformation, which is clearly exhibited in the third measurement. Figure 4c shows that the silver nanocystal was severely distorted from its initial cubic shape but elongated along the [1$\bar{1}$1] direction. For face centered cubic crystals, slip deformation usually occurs in the close packed {111} plane, which is consistent with our observation. The single nanocrystal has split into two disconnected pieces. These two fragments contain well-defined Bragg electron density, which implies that they shared the same crystalline structures and were aligned with the measurement [111] Bragg peak direction. This is a strong evidence for deformation twinning, where the remaining pieces were the distorted parent crystal. The twin domain was spun to the mirrored crystalline orientation and left a missing Bragg electron density in the reconstructed image.[35]

DOI: 10.1021/acs.nanolett.5b03568
Nano Lett. 2015, 15, 7644–7649

Figure 5a shows the central (110) cutplane of the reconstructed phases from the third measurement. The averaged phases and phase variations inside two remaining pieces are 0.17 ± 0.13 radians and 1.98 ± 0.08 radians, respectively. The relatively low variation (given by the error bar) indicates that the phases were quite uniform inside the two crystal fragments. The phase offset of 1.81 ± 0.15 radians between these two pieces was caused by a deformation along the $\mathbf{u}_{[1\bar{1}1]}$ direction and projected onto the $\mathbf{Q}_{[111]}$ direction. This phase offset is close to $2\pi/3$ which is caused by a deformation twinning with a width of $(3n + 2)d_{\{111\}}$, where $d_{\{111\}}$ is the lattice spacing between the silver {111} planes, as shown in Figure 5b. The other two phase offsets from $3n{\cdot}d_{\{111\}}$ and $(3n + 1)d_{\{111\}}$ are shown in Figure S3. Since deformation twinning usually occurs simultaneously with dislocation slip, so the coherent interface may not be perfectly flat, but distorted or curved, which could explain the difference between the measured 1.81 ± 0.15 radians and the expected $2\pi/3$ (2.09 radians) phase offset.

We noted that the plastic deformation continued on this silver nanocrystal. As shown in Figure 4d, in the fourth measurement conducted 75 min later, only one piece of the separated crystal retained its Bragg electron density aligned with the [111] direction, while the other piece must have rotated away and become undetectable with the measurement on the [111] direction. The evolution of the crystal volume is shown in Figure S4. It remained almost constant in the early stage of the deformation for the first two measurement. When the deformation twinning occurred, the crystal volume was decreased to about 64%. The volume of the larger piece of the split crystal had stabilized and remained nearly unchanged during the last measurement.

In conclusion, an external stress introduced evolution of crystal morphology and lattice distortion of a silver nanocube have been visualized in 3D with sequential Bragg CDI measurements conducted at 2.1 GPa. The nanocrystal was embedded in a solid Ice-VII phase inside a DAC. A slip deformation, deduced from the recovered phase distribution, was confirmed by its altered reconstructed shape. A deformation twinning with $(3n + 2)d_{\{111\}}$ width was observed during this plastic deformation process. This method provides a unique in situ approach to study a nanocrystal's response to external stress. It will facilitate the understanding and interoperation of the deformation mechanism of nanocrystals and thus provide characterization tool to boost the rational design and tuning properties of nanomaterials.

■ ASSOCIATED CONTENT

Supporting Information

The Supporting Information is available free of charge on the ACS Publications website at DOI: 10.1021/acs.nanolett.5b03568.

Details of sample preparation, data acquisition, and data analysis (PDF)

■ AUTHOR INFORMATION

Corresponding Authors

*E-mail: xjhuang@bnl.gov.

*E-mail: yangwg@hpstar.ac.cn.

Notes

The authors declare no competing financial interest.

■ ACKNOWLEDGMENTS

This work was supported by DOE-BES X-ray Scattering Core Program under grant number DE-FG02-99ER45775 and NSAF (Grant No. U1530402). Work at the National Synchrotron Light Source II, Brookhaven National Laboratory, was supported by the U.S. Department of Energy, Office of Science, Office of Basic Energy Sciences, under Contract No. DE-SC0012704. I.K.R. is supported by the ERC "nano-sculpture" advanced grant 227711. The measurements were carried out at APS beamline 34-ID-C, built with US National Science Foundation grant DMR-9724294 and operated by the US Department of Energy, Office of Basic Energy Sciences, under contract no. DE-AC0206CH11357.

■ REFERENCES

(1) Guillaume, C.; Gregoryanz, E.; Degtyareva, O.; McMahon, M.; Hanfland, M.; Evans, S.; Guthrie, M.; Sinogeikin, S.; Mao, H. *Nat. Phys.* **2011**, *7*, 211−214.

(2) Sun, L.; et al. *Nature* **2012**, *483*, 67−69.

(3) Somayazulu, M.; Dera, P.; Goncharov, A.; Gramsch, S.; Liermann, P.; Yang, W.; Liu, Z.; Mao, H.; Hemley, R. *Nat. Chem.* **2010**, *2*, 50−53.

(4) Eremets, M.; Troyan, I. *Nat. Mater.* **2011**, *10*, 927−931.

(5) Tolbert, S.; Alivisatos, A. *Science* **1994**, *265*, 373−376.

(6) Gu, Q.; Krauss, G.; Steurer, W.; Gramm, F.; Cervellino, A. *Phys. Rev. Lett.* **2008**, *100*, 045502.

(7) Yu, Q.; Shan, Z.; Li, J.; Huang, X.; Xiao, L.; Sun, J.; Ma, E. *Nature* **2010**, *463*, 335−338.

(8) Schiotz, J.; Tolla, F. D.; Jacobsen, K. *Nature* **1998**, *391*, 561−563.

(9) Chen, M.; Ma, E.; Hemker, K.; Sheng, H.; Wang, Y.; Cheng, X. *Science* **2003**, *300*, 1275−1277.

(10) Wang, L.; Liu, P.; Guan, P.; Yang, M.; Sun, J.; Cheng, Y.; Hirata, A.; Zhang, Z.; Ma, E.; Chen, M.; Han, X. *Nat. Commun.* **2013**, *4*, 2413.

(11) Pfeifer, M.; Williams, G.; Vartanyants, I.; Harder, R.; Robinson, I. *Nature* **2006**, *442*, 63−66.

(12) Robinson, I.; Harder, R. *Nat. Mater.* **2009**, *8*, 291−298.

(13) Yang, W.; Huang, X.; Harder, R.; Clark, J.; Robinson, I.; Mao, H. *Nat. Commun.* **2013**, *4*, 1680.

(14) Kamb, B. *Science* **1965**, *150*, 205−209.

(15) Mishima, O.; Endo, S. *J. Chem. Phys.* **1980**, *73*, 2454.

(16) Poirier, J.; Sotin, C.; Peyronneau, J. *Nature* **1981**, *292*, 225.10.1038/292225a0

(17) Liang, M.; Harder, R.; Robinson, I. *IUCrJ* **2014**, *1*, 172−178.

(18) Huang, Z.; Bartels, M.; Xu, R.; Osterhoff, M.; Kalbfleisch, S.; Sprung, M.; Suzuki, A.; Takahashi, Y.; Blanton, T.; Salditt, T.; Miao, J. *Nat. Mater.* **2015**, *14*, 691−695.

(19) Sun, Y.; Xia, Y. *Science* **2002**, *298*, 2176−2179.

(20) Huang, X.; Wojcik, M.; Burdet, N.; Peterson, I.; Morrison, G.; Vine, D.; Legnini, D.; Harder, R.; Chu, Y.; Robinson, I. K. *Opt. Express* **2012**, *20*, 24038−24048.

(21) Mineev, V.; Funtikov, A. *High Temp.* **2005**, *43*, 141−150.

(22) Shimizu, H.; Nabetani, T.; Nishiba, T.; Sasaki, S. *Phys. Rev. B: Condens. Matter Mater. Phys.* **1996**, *53*, 6107−6110.

(23) Takahashi, Y.; Nishino, Y.; Ishikawa, T. *Phys. Rev. A: At., Mol., Opt. Phys.* **2007**, *76*, 033822.

(24) Williams, G.; Pfeifer, M.; Vartanyants, I.; Robinson, I. *Phys. Rev. Lett.* **2003**, *90*, 175501.

(25) Gerchberg, R.; Saxton, W. *Optik* **1972**, *35*, 237.

(26) Fienup, J. *Opt. Lett.* **1978**, *3*, 27−29.

(27) Fienup, J. *Appl. Opt.* **1982**, *21*, 2758−2769.

(28) Marchesini, S.; He, H.; Chapman, H.; Hau-Riege, S.; Noy, A.; Howells, M.; Weierstall, U.; Spence, J. *Phys. Rev. B: Condens. Matter Mater. Phys.* **2003**, *68*, 140101.

(29) Clark, J.; Huang, X.; Harder, R.; Robinson, I. *Nat. Commun.* **2012**, *3*, 993.

(30) Henderson, R.; Moffat, J. *Acta Crystallogr., Sect. B: Struct. Crystallogr. Cryst. Chem.* **1971**, *B27*, 1414−1420.

DOI: 10.1021/acs.nanolett.5b03568
Nano Lett. 2015, 15, 7644−7649

(31) Watari, M.; McKendry, R.; Vogtli, M.; Aeppli, G.; Soh, Y.; Shi, X.; Xiong, G.; Huang, X.; Harder, R.; Robinson, I. *Nat. Mater.* **2011**, *10*, 862−866.
(32) Kittel, C. *Introduction to Solid State Physics*, 8th ed.; Wiley: New York, 2004.
(33) Kaye, G.; Laby, T. *Tables of Physical and Chemical Constants*, 15th ed.; Longmans: London, 1993.
(34) Mackenzie, D.; Boyle, J. *Int. J. Pressure Vessels Piping* **1992**, *53*, 77−95.
(35) Ulvestad, A.; Clark, J.; Harder, R.; Robinson, I.; Shpyrko, O. *Nano Lett.* **2015**, *15*, 4066−4070.

DOI: 10.1021/acs.nanolett.5b03568
Nano Lett. 2015, 15, 7644−7649